Perturbative treatments of pump–probe laser-molecule interactions with applications to azulene and trimethylazulene

Phuc Tran[a),b)] and William J. Meath[b)]
Department of Chemistry, University of Western Ontario, London, Ontario N6A 5B7, Canada

Brian D. Wagner[c)] and Ronald P. Steer
Department of Chemistry, University of Saskatchewan, Saskatoon, Saskatchewan S7N 0W0, Canada

(Received 13 October 1993; accepted 1 December 1993)

Semianalytic perturbative approaches for investigating the spectroscopy, and the underlying dynamics, associated with fast time-resolved, two-photon, two-color, pump–probe, low intensity laser-molecule interactions are developed and discussed. In particular the perturbation theory is developed with emphasis on molecular models associated with pump–probe experiments on the $S_0 \rightarrow S_1 \rightarrow S_2$ two-photon transitions in azulene and trimethylazulene. The experiments are discussed and the theory is used to determine the lifetimes of the intermediate S_1 states by analyzing the experimental two-photon fluorescence signals from the S_2 states as a function of the time-delay between the pump and probe lasers. The advantages of using this approach relative to the traditional methods for determining the lifetime of the S_1 states are discussed. The dependence of the two-photon fluorescence signals on the angle between the polarization vectors of the pump and probe lasers, for fixed time delay between the lasers, is also considered briefly.

I. INTRODUCTION

Pump–probe methods have frequently been used to investigate the dynamics of the S_1 states of azulene and other nonalternant aromatic hydrocarbons in solution.[1–5] In this paper semianalytic perturbative approaches for investigating the spectroscopy, and the underlying dynamics, associated with fast time-resolved, two-photon, two-color, pump–probe, low intensity laser-molecule interactions are discussed with particular reference to recent[4,5] and current experiments involving two-photon excited $S_2 \rightarrow S_0$ fluorescence of azulene and trimethylazulene.

The perturbation theory is outlined in Sec. II with particular emphasis on the theory and few-level models associated with pump–probe experiments on the $S_0 \rightarrow S_1 \rightarrow S_2$ two-photon transitions in azulene (Sec. II A) and trimethylazulene (Sec. II B). The experiments themselves are discussed briefly in Sec. III. Applications to the determination of the lifetimes of the intermediate S_1 states, by using the theory and models to analyze the experimental two-photon fluorescence signals from the S_2 states as a function of the time-delay between the pump and probe lasers, are discussed in Sec. IV A. This approach offers an alternative to traditional methods[4] which use pulse correlation techniques such as two-photon excited $S_1 \rightarrow S_0$ fluorescence of laser dyes or second harmonic generation in an appropriate nonlinear crystal to generate the required instrument response function. The theory/models of Sec. II predicts that the two-photon fluorescence signals from the S_2 state of azulene and trimethylazulene are proportional to $\cos^2\theta$, where θ is the angle between the polarization vectors of the pump and probe lasers, for fixed time delay between the lasers. This is in agreement with experiment, as illustrated in Sec. IV B for zero time delay between the lasers. Section V contains a brief discussion of some of the more general features and implications of this work.

II. THEORY AND MODELS

Here expressions for the relevant excited state populations are derived using semiclassical radiation theory in the perturbative regime.

The time-dependent wave function for the interaction of a molecule with a time-dependent perturbation $V(t)$ can be written as[6–8]

$$\Psi = \left[\sum_{l=1}^{\infty} b_l(t) \psi_l \exp(-iE_l t/\hbar) \right] \times \exp\left[-\frac{i}{\hbar} \int_{-\infty}^{t} V_{11}(t')dt' \right], \tag{1}$$

where ψ_l and E_l are the time-dependent wave function and energy of the lth stationary state of the molecule, and $V_{lk}(t) = \langle \psi_l | V(t) | \psi_k \rangle$ and we assume $V(-\infty) = 0$. The interaction representation defined by Eq. (1) is particularly useful for dealing with the effects of permanent dipoles[7–9] on multiphoton transitions from the ground ($l = 1$) state.

The state amplitudes can be expanded perturbatively to obtain[6,7]

$$b_l(t) = \sum_{n=0}^{\infty} b_l^{(n)}(t) \tag{2}$$

and the $b_l^{(n)}(t)$ satisfy the coupled differential equations given by

[a)] Present address: Naval Air Warfare Center-Weapons Division, China Lake, California 93555.
[b)] Associated with the Center for Interdisciplinary Studies in Chemical Physics, University of Western Ontario, London, Ontario, Canada N6A 5B7.
[c)] Present address: Steacie Institute for Molecular Sciences, National Research Council of Canada, Ottawa, Canada K1A 0R6.

 0021-9606/94/100(6)/4165/6/$6.00

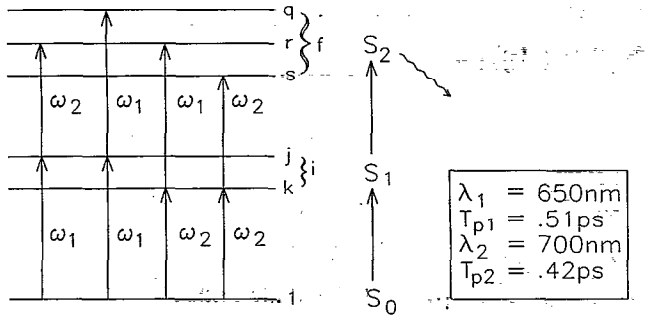

FIG. 1. Model for the TPF for azulene. The relevant states S_0, S_1, and S_2 are represented by one(1), two (j,k), and the three levels (q,r,s), respectively, under the assumptions discussed in the main text. The relevant experimental laser wavelengths and pulse widths are also indicated on the figure.

$$\frac{d}{dt}b_l^{(n)}=-\frac{i}{\hbar}\sum_{m=1}^{\infty}\langle\psi_l|\hat{V}(t)|\psi_m\rangle b_m^{(n-1)}\exp\left[\frac{i}{\hbar}(E_l-E_m)t\right] \tag{3}$$

$$\hat{V}(t)=V(t)-V_{11}(t)=-(\boldsymbol{\mu}-\boldsymbol{\mu}_{11})\cdot\mathbf{E}(t) \tag{4}$$

since, for the problems of interest here, $V(t)=-\boldsymbol{\mu}\cdot\mathbf{E}(t)$, where $\boldsymbol{\mu}$ is the electric dipole moment operator for the molecule and $\boldsymbol{\mu}_{11}$ is the permanent dipole of the ground state. For the applications considered later, the electric field $\mathbf{E}(t)$ is given by

$$\mathbf{E}(t)=\hat{e}_1E_1F_1(t)\cos\omega_1t+\hat{e}_2E_2F_2(t-t_d)\times\cos[\omega_2(t-t_d)+\delta], \tag{5}$$

where $\hat{e}_i$, E_i, F_i, and ω_i are the polarization vector, electric field strength, pulse envelope, and circular frequency of the ith laser, while t_d and δ are the time delay and the phase difference between the two pulses.

We now consider two-photon processes related to two, few-level, molecular models which can be used to analyze two-photon fluorescence data from pump–probe experiments. For initial conditions $b_l(-\infty)=\delta_{l1}$, the amplitude for two-photon absorption from the ground state, 1, to the final state, f, which can involve intermediate states $l\neq1,f$, is easily obtained by iteration on Eq. (3),

$$b_f^{(2)}(t)=\left(-\frac{i}{\hbar}\right)^2\sum_{m=1}^{\infty}\int_{-\infty}^{t}\hat{V}_{fm}(t')\exp\left[\frac{i}{\hbar}(E_f-E_m)t'\right]\times\int_{-\infty}^{t'}\hat{V}_{m1}(t'')\exp\left[\frac{i}{\hbar}(E_m-E_1)t''\right]dt''dt'. \tag{6}$$

A. Six-level model (azulene: $S_0\rightarrow S_1\rightarrow S_2$)

The model is illustrated in Fig. 1 and is chosen to represent the $S_0\rightarrow S_1\rightarrow S_2$ two-photon transition in azulene which involves intermediate states j and k. Substituting Eqs. (4) and (5) into Eq. (6), making use of $\cos(\omega t)=(1/2)(e^{i\omega t}+e^{-i\omega t})$, neglecting off-resonance terms (which involve rapidly oscillating time dependencies e^{iat} with $a\neq0$) and the effects of permanent dipoles (which are small for this problem), the amplitude for excitation can be written as

$$\begin{aligned}b_f^{(2)}(t)=\left(-\frac{i}{2\hbar}\right)^2[&E_2E_1(\boldsymbol{\mu}_{rj}\cdot\hat{e}_2)(\boldsymbol{\mu}_{1j}\cdot\hat{e}_1)Q_{21}(1\rightarrow j\rightarrow f)\\&\times\exp(i\Delta)+E_1E_2(\boldsymbol{\mu}_{rk}\cdot\hat{e}_1)(\boldsymbol{\mu}_{1k}\cdot\hat{e}_2)Q_{12}(1\rightarrow k\rightarrow f)\\&\times\exp(i\Delta)+E_1^2(\boldsymbol{\mu}_{qj}\cdot\hat{e}_1)(\boldsymbol{\mu}_{1j}\cdot\hat{e}_1)Q_{11}(1\rightarrow j\rightarrow f)\\&+E_2^2(\boldsymbol{\mu}_{sk}\cdot\hat{e}_2)(\boldsymbol{\mu}_{1k}\cdot\hat{e}_2)Q_{22}(1\rightarrow k\rightarrow f)\exp(2i\Delta)]\end{aligned} \tag{7}$$

$$Q_{nm}(1\rightarrow p\rightarrow f)=\int_{-\infty}^{t}F_n(t')\int_{-\infty}^{t'}F_m(t'')\exp\left[-\frac{1}{2\tau}(t'-t'')\right]dt''dt', \tag{8}$$

where $\Delta=\omega_2t_d-\delta$, $F_2(t)=F_2(t-t_d)$ and τ is the lifetime of the intermediate state ($E_i\rightarrow E_i-i/2\tau$), which is introduced in these results phenomenologically. The corresponding probability of excitation to state f is given by $|b_f^{(2)}(t)|^2$. Assuming the effective phase Δ is random, and that the absorbing molecules are randomly oriented, the physically meaningful probability of excitation is given by the phase ($0\leqslant\Delta\leqslant2\pi$) and orientational average of $|b_f^{(2)}(t)|^2$,

$$\begin{aligned}\overline{|b_f^{(2)}(t)|^2}=\frac{1}{16\hbar^4}\{&E_1^2E_2^2[\langle(\boldsymbol{\mu}_{fi}\cdot\hat{e}_2)^2(\boldsymbol{\mu}_{1i}\cdot\hat{e}_1)^2\rangle Q_{21}^2\\&+\langle(\boldsymbol{\mu}_{fi}\cdot\hat{e}_1)^2(\boldsymbol{\mu}_{1i}\cdot\hat{e}_2)^2\rangle Q_{12}^2+2\langle(\boldsymbol{\mu}_{fi}\cdot\hat{e}_1)\\&\times(\boldsymbol{\mu}_{1i}\cdot\hat{e}_2)(\boldsymbol{\mu}_{fi}\cdot\hat{e}_2)(\boldsymbol{\mu}_{1i}\cdot\hat{e}_1)\rangle Q_{21}Q_{12}]\\&+E_1^4\langle(\boldsymbol{\mu}_{fi}\cdot\hat{e}_1)^2(\boldsymbol{\mu}_{1i}\cdot\hat{e}_1)^2\rangle Q_{11}^2\\&+E_2^4\langle(\boldsymbol{\mu}_{fi}\cdot\hat{e}_2)^2(\boldsymbol{\mu}_{1i}\cdot\hat{e}_2)^2\rangle Q_{22}^2\}.\end{aligned} \tag{9}$$

Here we have assumed that $\boldsymbol{\mu}_{rj}=\boldsymbol{\mu}_{rk}=\boldsymbol{\mu}_{qj}=\boldsymbol{\mu}_{sk}=\boldsymbol{\mu}_{fi}$ and $\boldsymbol{\mu}_{1j}=\boldsymbol{\mu}_{1k}=\boldsymbol{\mu}_{1i}$, and in Eq. (9) the brackets $\langle\ \rangle$ denote orientational averaging. Carrying out the orientational averages, using methods analogous to those already discussed[7,10] in the literature, yields

$$\begin{aligned}\overline{|b_f^{(2)}(t)|^2}=\frac{\mu_{fi}^2\mu_{1i}^2}{16\hbar^4}\{&E_1^2E_2^2[(Q_{21}^2+Q_{12}^2)B(\alpha,\theta)\\&+2Q_{21}Q_{12}C(\alpha,\theta)]+[E_1^4Q_{11}^2+E_2^4Q_{22}^2]A(\alpha)\},\end{aligned} \tag{10}$$

where

$$A(\alpha)=\frac{1}{15}(1+2\cos^2\alpha), \tag{11}$$

$$B(\alpha,\theta)=\frac{1}{15}[(3\cos^2\theta-1)\cos^2\alpha+2-\cos^2\theta], \tag{12}$$

$$C(\alpha,\theta)=\frac{1}{30}[(3+\cos^2\theta)\cos^2\alpha+3\cos^2\theta-1], \tag{13}$$

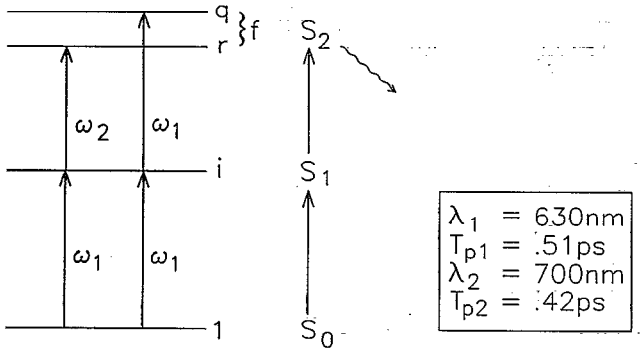

FIG. 2. Model for the TPF for TMA. The relevant states S_0, S_1, and S_2 are represented by one(1), one (i), and two levels (q,r), respectively. The relevant experimental laser wavelengths and pulse widths are also indicated on the figure.

where α is the angle between $\boldsymbol{\mu}_{1i}$ and $\boldsymbol{\mu}_{fi}$ and θ is the angle between the polarization vectors $\hat{e}_1$ and $\hat{e}_2$. For $\hat{e}_1=\pm\hat{e}_2$, $A(\alpha)=B(\alpha,\theta=0 \text{ or } \pi)=C(\alpha,\theta=0 \text{ or } \pi)$.

B. Four-level model (trimethylazulene: $S_0 \rightarrow S_1 \rightarrow S_2$)

The model is illustrated in Fig. 2 and is chosen to represent the $S_0 \rightarrow S_1 \rightarrow S_2$ two photon, two-color transition in trimethylazulene (TMA). In contradistinction to the model for the pump–probe excitation of azulene (Fig. 1), here only laser *1*, having circular frequency ω_1, can induce transitions to the intermediate level i since $\hbar\omega_2$ is below the absorption threshold for the $1 \rightarrow i$ transition. The derivation of the phase and orientationally averaged transition probability for excitation to the final stage f follows from that for the azulene model and the result for TMA is given by Eq. (10) with Q_{22} and Q_{12} both zero,

$$|b_f^{(2)}(t)|^2=\frac{\mu_{fi}^2\mu_{1i}^2}{16\hbar^2}\,[E_1^4Q_{11}^2A(\alpha)+E_1^2E_2^2Q_{21}^2B(\alpha,\theta)]. \tag{14}$$

III. EXPERIMENT

A schematic diagram of the experimental pump–probe setup is shown in Fig. 3. The frequency-doubled output of a pulse-compressed, mode-locked Nd:YAG laser is used to synchronously pump two fs dye lasers, one using DCM dye (the pump), the other using pyridine-1 (the probe). This arrangement allows for the independent variation of the pump and probe wavelengths and polarizations, at the expense of reduced time resolution due to jitter. The pump beam is passed through an optical delay line consisting of a fixed mirrored right angle prism and a retroreflector mounted on a translation stage. The probe beam is passed through a polarization rotator consisting of a fresnel double rhomb mounted on a 360° rotation stage. The pump and probe beams are collinearly counterpropagated and focused onto a 0.1 mm path length quartz cell containing the sample solution. The emission from the sample is collected and is focused onto a photomultiplier tube. Full details of this experimental setup have been given elsewhere.[4]

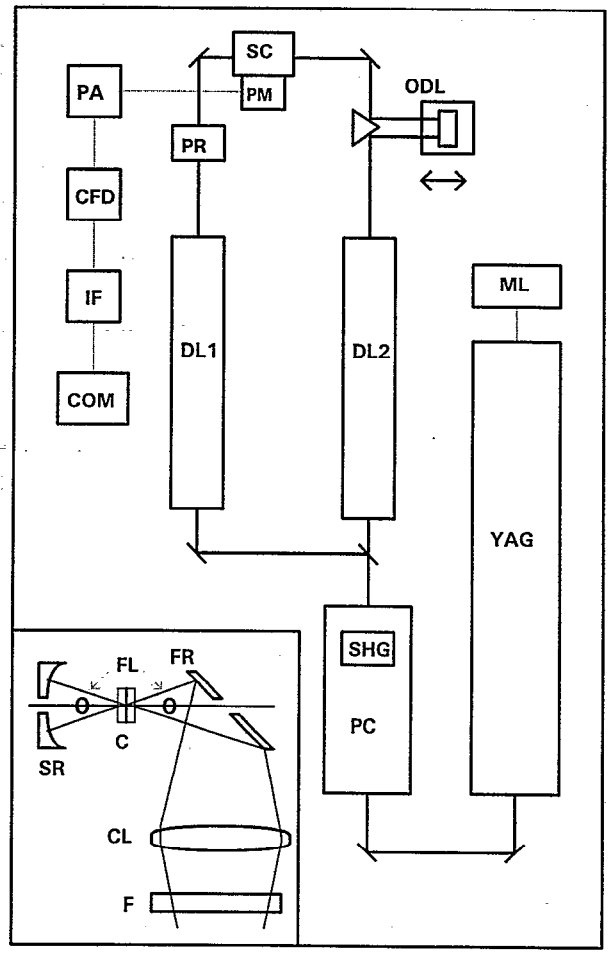

FIG. 3. Schematic diagram of the experimental setup (reproduced from Ref. 4). YAG, Nd:YAG laser; ML, 41 MHz mode locker; PC, IR fiber optic pulse compressor; SHG, second harmonic generation assembly; DL1,2, fs dye lasers; ODL, optical delay line; PR, polarization rotator; SC, sample chamber; PM, photomultiplier tube; PA, preamplifier; CFD, constant fraction discriminator; IF, IEEE-488 interface; COM, computer. (Inset) The optical configuration of the sample chamber. SR, spherical reflector; FL, focusing lenses; C, sample cell; FR, flat reflector; CL, condensing lens; F, filters (to remove the scattered pump and probe beams).

The (intensity) output dye laser pulses have a sech^2 shape, with a full-width at half-maximum (FWHM) of 0.4–0.6 ps as measured by the autocorrelation technique.[11] The FWHM of the cross-correlation function of these two lasers was measured to be 2.0–2.6 ps. This cross-correlation FWHM can be related to the dye laser pulse widths and the relative temporal jitter between them by the following working expression:

$$\text{FWHM}_{CC}^2=\text{FWHM}_{DL1}^2+\text{FWHM}_{DL2}^2+(\text{jitter})^2. \tag{15}$$

From this expression and the values of FWHM_{CC} and the dye laser pulse widths, it can be determined that the jitter is the major contributing factor to the measured cross-correlation width.

Two types of experiments were performed. In the first type ("translation scan"), the optical path length of the pump beam was varied using the adjustable optical delay

line, which allowed for the control of the relative time delay between the arrival at the sample of the pump and probe pulses. The intensity of the S_2 fluorescence was measured as a function of the relative time delay. In the second type ("rotation scan"), the pump and probe path lengths were fixed and equal, and the polarization of the probe beam was varied using the polarization rotator. The intensity of the S_2 fluorescence was measured as a function of the relative angle between the polarization of the pump and probe pulses. In both cases, ten individual fluorescence intensity readings were averaged at each translation or rotation stage position.

Azulene (Aldrich) was used as received. 4, 6, 8-Trimethylazulene (TMA) was synthesized and purified according to the method of Garst *et al.*[12] Cyclohexane (CH; BDH Omnisolv) was fractionally distilled before use. The solutions were 10^{-3}–10^{-2} M in concentration.

IV. APPLICATIONS OF THEORY/MODELS TO PUMP–PROBE TPF EXPERIMENTS

A. Determination of intermediate state lifetimes

One application of the theory and models of Sec. II is to the analysis of two-photon fluorescence (TPF) data to determine the lifetime of an intermediate state. A pump–probe setup (Sec. III) is particularly attractive if the intermediate state has low fluorescence. The pump pulse induces population transfer to the state of interest and the probe pulse, separated from the first pulse by a time delay t_d, then induces a transition from this state to a state with high fluorescence yield that is readily measured. This fluorescence $I(t_d)$, as a function of t_d, can be analyzed to give the lifetime of the intermediate state.

Depending on the molecule, TPF experiments of this type can be modeled by the six- and four-level systems discussed in Secs. II A and II B or by analogous few-level models. The $S_2 \rightarrow S_0$ fluorescence intensity observed in each case is proportional to the probability of sequential excitation to state f after the pump and probe pulses have passed through the system [operationally for $t \geqslant 4\times$ (pulse widths) $= \infty$]. Under the experimental conditions of interest here (see below and Sec. III, Ref. 4), the appropriate measure of TPF is the phase and orientationally averaged probability of excitation to state f, namely $\overline{|b_f^{(2)}(\infty)|^2}$.

The approaches and procedures described in Sec. III have been used to determine the S_1 lifetimes of azulene and TMA in cyclohexane. With $\hat{e}_1 = \hat{e}_2$ the pump–probe system was used to induce the $S_0 \rightarrow S_1 \rightarrow S_2$ transition and the fluorescence from S_2 was detected as a function of t_d. The wavelengths (λ_i) and pulse widths (T_{p_i}), and the TPF signals I as a function of t_d, are given in Figs. 1 and 4, and 2 and 5, for the azulene and TMA experiments, respectively. In each case the constant background due to two-photon, one-color fluorescence and noise has been subtracted and the results normalized to the maximum value of the TPF [i.e., the quantity plotted is $I(t_d)/I(t_d)_{\max}$]; the maximum value for $I(t_d)$ occurs at $t_d = 0$ for azulene and at $t_d > 0$ for TMA. The data from the experiments are a sum of the results from a sequence of many pump–probe pulses at a repetition rate of ≈ 82 MHz.

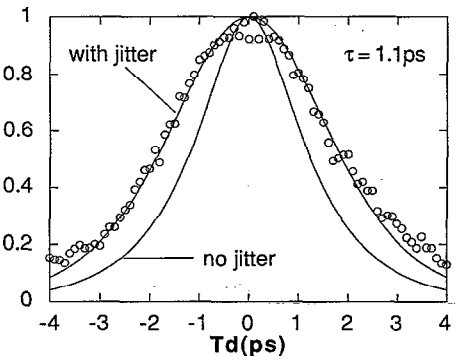

FIG. 4. TPF signal for azulene as a function of t_d for $\hat{e}_1 = \hat{e}_2$. ○, experimental; —, theory with $\tau = 1.1$ ps both with and without jitter.

To connect the theory with experiment one must include a function in the calculations which represents the experimental jitter in the time delay. The experimental pulse sequences have a distribution of delay times (jitter) centered about the desired time delay, and the TPF signal as function of t_d is broadened because of this effect. The TPF signal, $I(t_d)$, is then proportional to the theoretical results of Sec. II weighted by a Gaussian distribution function which has been chosen to represent the jitter;

$$I(t_d) \alpha \int_{-\infty}^{\infty} \overline{|b_f^{(2)}(\infty, t_d')|^2} \exp[-(t_d - t_d')^2 / T_J^2] dt_d'. \tag{16}$$

For the experiments reported here $F_i(t) = \operatorname{sech}(t/T_{p_i})$ and the jitter is characterized by $T_J = 1.4$ ps. The field strengths E_i are very weak (average power ≈ 100 mW, peak power ≈ 1 kW), and the pulse durations are short, so the perturbation theory used to derive the results in Sec. II is applicable. The calculations are carried out with the background terms in $\overline{|b_f^{(2)}(\infty)|^2}$ deleted (these are the Q_{ii} which are independent of t_d since they correspond to two-photon absorption from the same pulse). The theoretical results are reported as $I(t_d)/I(t_d)_{\max}$ so that the field

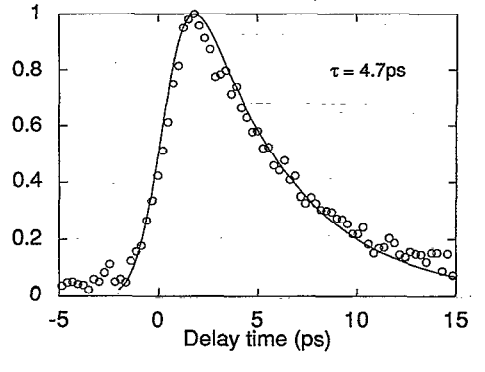

FIG. 5. TPF signal for TMA as a function of t_d for $\hat{e}_1 = \hat{e}_2$. ○, experimental; —theory with $\tau = 4.7$ ps including jitter.

strengths and the molecular transition dipoles occurring in our results for $\overline{|b_f^{(2)}(\infty)|^2}$ cancel. The required integrals Q_{nm}, defined by Eq. (8), are evaluated using the Gauss–Kronrod method and the IMSL subroutine[13] TWODQ. The so-called "coherent artifact" (for example, Refs. 3 and 14), which is due to coherence of the pump and probe pulses in one-laser, two-photon, one-color experiments, is included in the theory as appropriate.

1. Azulene (model of Fig. 1)

The theoretical result obtained using Eq. (16), with $\overline{|b_f^{(2)}(\infty,t_d')|^2}$ based on the model of Fig. 1 and the theory outlined in Sec. II A, is fit (see Fig. 4) to the experimental data to give $\tau=1.1$ ps. The traditional procedure for extracting intermediate state lifetimes from pump–probe experiments involves deconvolution of the measured fluorescence intensity vs t_d curve for the sample using an experimentally measured instrument response function. The latter is often generated by measuring the TPF intensity vs t_d for laser dyes such as α-NPO (2-[1-naphthyl]-5-phenyloxazole) in which the S_1 state is populated directly by two-photon absorption. Using this traditional procedure Wagner *et al.*[4] obtained $\tau=1.1$ ps from an analysis of the same data as displayed in Fig. 4, in perfect agreement with the theoretical result given above. By analyzing 15 such data sets, Wagner *et al.*[4] obtained $\tau_{av}=1.03\pm0.10$ ps in good agreement with the value of Schwarzer *et al.*,[3] $\tau_{av}=1.0\pm0.1$ ps, who also used the traditional deconvolution procedure. Figure 4 also shows our theoretical result with the jitter omitted, thus illustrating the importance of including this effect in the analysis of TPF time delay data.

2. Trimethylazulene (model of Fig. 2)

The theoretical result Eq. (16), with $\overline{|b_f^{(2)}(\infty,t_d')|^2}$ based on the model of Fig. 2 and the theory outlined in Sec. II B, is fit (Fig. 5) to experiment to give $\tau=4.7$ ps which is in good agreement with the result $\tau=4.5$ ps obtained by Wagner *et al.*[4] from the experimental data of Fig. 5 using the traditional method referred to in Sec. IV A 1. Averaging six such values of τ, Wagner *et al.*[4] obtained $\tau_{av}=4.0\pm0.3$ ps for TMA in CH. Only the pump laser ($\lambda_1=630$ nm) can promote the $S_0\rightarrow S_1$ transition in TMA leading to the "asymmetrical" TPF time delay results of Fig. 5 in comparison with the "symmetric" results obtained for azulene in Fig. 4.

B. Polarization effects on TPF

The TPF signal depends on the time delay between the pump and probe pulses *and* on the angle θ between the polarization vectors $\hat{e}_1$ and $\hat{e}_2$ of the two pulses. For $t_d=0$, experimental TPF signals for azulene and TMA are shown in Figs. 6 and 7, respectively, as a function of θ; backgrounds have been subtracted and the curves are normalized to their maximum value as a function of θ.

For fixed t_d, the theory of Secs. II A and II B predicts that the TPF signal for both azulene and TMA should be proportional to $\cos^2\theta$ and this is the case, within experimental uncertainty, as illustrated in Figs. 6 and 7 (the solid line is $\cos^2\theta$).

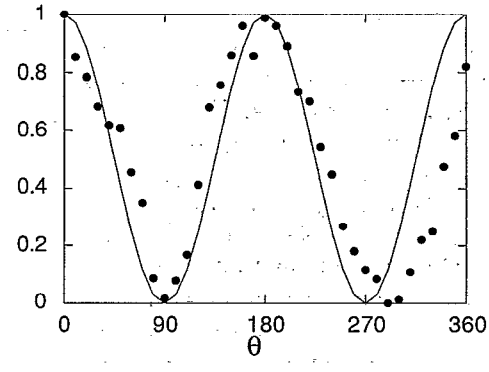

FIG. 6. TPF signal for azulene as a function of θ for $t_d=0$. ●, experimental; —, $\cos^2\theta$ normalized to highest experimental value (see main text).

V. COMMENTS

Perturbation theory expressions, based on few-level molecular models, for laser-molecule interactions can be used to model fluorescence from excited states due to two-color, pump–probe laser excitations and to determine lifetimes of intermediate states without using traditional methods. This is illustrated in Secs. II and IV for the TPF of both azulene and TMA as a function of time delay for fixed polarization of the two pulses and as a function of polarization for fixed time delay.

Traditional methods of extracting the lifetimes of intermediate states from time-resolved (sub)picosecond pump–probe fluorescence involve "deconvolution" of a measured instrument response function (IRF) from the measured I vs t_d profile for the sample. This is achieved by assuming a functional form for the decay of the intermediate state population (monoexponential) and then finding, by iteration, the lifetime which, when convoluted with the IRF, gives the "best fit" to the measured I vs t_d data. The IRF must be measured experimentally by a pulse cor-

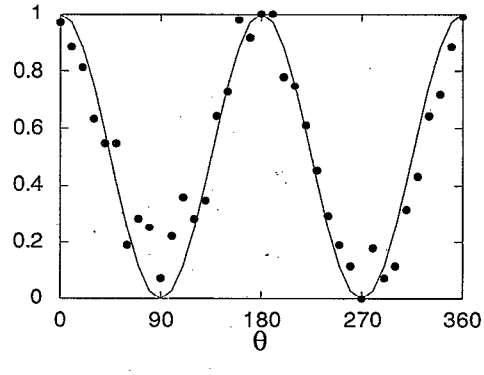

FIG. 7. TPF signal for TMA as a function of θ for $t_d=0$. ●, experimental; —, $\cos^2\theta$ normalized to highest experimental value.

relation method involving the generation of either $S_1 \rightarrow S_0$ fluorescence from a laser dye by a two-photon excitation or the second harmonic of the pump and probe beams in an appropriate nonlinear crystal. The data of experiments in which the output of a single mode-locked laser is split in order to produce pump and probe beams of identical wavelength have been analyzed in this way since the inception of the TPF pump–probe method.[1–5] Data from experiments in which two synchronously-pumped dye lasers are used to generate pump and probe beams of different colors can, in principle, be analyzed in a similar fashion,[4,5] but with the significant experimental complication that the IRF is broadened considerably by jitter in the two trains of pulses. When temporal jitter of an assumed (Gaussian) functional form is introduced into the analytical expressions developed herein for the TPF signals, excellent correspondence with the intermediate state lifetimes extracted by these traditional methods is obtained.

Using the perturbative formulas has several advantages over the methods of Refs. 1–5. The TPF signal is given explicitly in terms of the molecular parameters and therefore one can obtain information regarding these molecular parameters (for example dipole moments and their relative orientation). Also, for example, the perturbative treatments can be used to analyze systems with equally (azulene) and nonequally (TMA) spaced energy levels in a consistent manner.

The perturbation theory results are analytical expressions involving the parameters characterizing both the laser and the molecule. Expressions of this type should be useful in investigations of the dynamics and spectroscopy associated with various laser pump–probe molecular excitation schemes, as a function of these parameters, including phase, for weak laser intensities. The combination of experiment and these perturbative results can be used to give information about molecular properties for situations where the absorbing molecule has a fixed orientation relative to the applied electromagnetic fields as well as for the orientationally averaged cases studied explicitly in this paper. For processes involving high intensity lasers and/or temporal behavior of molecular systems over long time periods, other methods are, of course, needed.

ACKNOWLEDGMENTS

We thank B. N. Jagatap for helpful discussions and D. Tittelbach-Helmrich for synthesizing the TMA. This research was supported by grants from the Canadian National Networks of Centers of Excellence through the Centers of Excellence in Molecular and Interfacial Dynamics (CEMAID).

[1] E. P. Ippen, C. V. Shank, and R. L. Woerner, Chem. Phys. Lett. **46**, 20 (1977).
[2] C. V. Shank, E. P. Ippen, O Teschke, and R. L. Fork, Chem. Phys. Lett. **57**, 433 (1978).
[3] D. Schwarzer, J. Troe, and J. Schroeder, Ber. Bunsenges. Phys. Chem. **85**, 933 (1991).
[4] B. D. Wagner, M. Szymanski, and R. P. Steer, J. Chem. Phys. **98**, 301 (1993).
[5] D. Tittelbach-Helmrich, B. D. Wagner, and R. P. Steer, Chem. Phys. Lett. **209**, 464 (1993).
[6] P. W. Langhoff, S. T. Epstein, and M. Karplus, Rev. Mod. Phys. **44**, 602 (1972).
[7] W. J. Meath and E. A. Power, J. Phys. B **17**, 763 (1984).
[8] W. J. Meath and E. A. Power, Mol. Phys. **51**, 585 (1984).
[9] S. Nakai and W. J. Meath, J. Chem. Phys. **96**, 4991 (1992), and references therein.
[10] R. A. Thuraisingham and W. J. Meath, Chem. Phys. **125**, 129 (1988).
[11] K. L. Sala, G. A. Kenney-Wallace, and G. E. Hall, IEEE J. Quantum Electron. **QE-16**, 990 (1980).
[12] M. E. Garst, J. Hochlowski, J. G. Douglass III, and S. Sasse, J. Chem. Ed. **60**, 510 (1983).
[13] Math/Library, 1987, Version 1.0, IMSL Inc., Houston, Texas, U.S.A.
[14] A. Laubereau, in *Ultrashort Laser Pulses and Applications*, edited by W. Kaiser (Springer, Berlin, 1988), p. 88.